https://doi.org/10.5194/egusphere-2026-1628
Preprint. Discussion started: 29 April 2026

High Frequency of Urban New Particle Formation on the Tibetan Plateau: Quantifying Formation Rates, Growth Rates, and CCN Production

Qiqi Mo[1], Longjie Wen[1,2], Gang Zhao[1,3*], Chunxiang Ye[4*], Jie Sun[1], Weili Lin[1,5], Fengjun Shen[1], Tong Liu[1], Yicheng Gao[1], Yi Chen[4], Tiantian Zhang[1], Tong Zhu[4]

1Key Laboratory of Ecology and Environment in Minority Areas, Minzu University of China, National Ethnic Affairs Commission, Beijing 100081, China
2School of Ecology and Environment, College of Intelligence, Harbin Institute of Technology (Shenzhen), Shenzhen, 518055, China
3Key Laboratory of Biodiversity and Environment on the Qinghai-Tibet Plateau, Ministry of Education, Xizang University, Lhasa 850000, China
4SKL-ESPC & SEPKL-AERM, College of Environmental Sciences and Engineering, Institute of Tibetan Plateau, and Center for Environment and Health, Peking University, Beijing, China
5Institute of National Security, Minzu University of China, Beijing, 100081, China

Correspondence to: Gang Zhao (gangz@muc.edu.cn) and Chunxiang Ye (c.ye@pku.edu.cn)

Abstract

New particle formation (NPF) strongly influences aerosol number size distributions and cloud condensation nuclei (CCN), yet its characteristics and climatic relevance in high-altitude urban environments over the Tibetan Plateau (TP) remain poorly constrained. We conducted in situ observations at Tibet University in Lhasa during the monsoon and pre-monsoon seasons. NPF event frequencies were 86.2 % during the monsoon season and 55.1 % during the pre-monsoon period. Observation days were classified into four types (Class I, Class II, Undefined, and Non-Event) based on the evolution of particle number size distribution (PNSD) and modal development. Seasonal comparisons indicate clear differences in the factors associated with NPF: monsoon season NPF was mainly associated with sulfur precursor availability, whereas no single clear controlling factor was evident during the pre-monsoon period. NPF substantially enhanced CCN at TU, with mean concentrations of 3351 ± 1919 cm^{-3} on Class I days, 1540.2 ± 872 cm^{-3} on Class II days, 880.5 ± 374 cm^{-3} on Undefined days, and 1278.1 ± 667 cm^{-3} on Non-Event days. The impact of NPF on CCN depends not only on nucleation, but also on the continued growth and survival of newly formed particles. This study provides new insights into urban NPF characteristics and the contribution of NPF to CCN on the TP, improving our understanding of aerosol–climate interactions in high-altitude urban environments.

https://doi.org/10.5194/egusphere-2026-1628
Preprint. Discussion started: 29 April 2026

1 Introduction

The Sixth Assessment Report of the Intergovernmental Panel on Climate Change (IPCC) highlights that the aerosol climatic effect is a major source of uncertainty in climate change assessment, primarily attributed to the spatio-temporal variability of aerosol concentration and size distribution (Arias et al., 2021). New Particle Formation (NPF) and subsequent particle growth significantly alter aerosol concentration, size distribution, and Cloud Condensation Nuclei (CCN) concentration (Hong et al., 2023). Endowed with unique geographical and atmospheric conditions, the Tibetan Plateau (TP) hosts aerosols that are prone to long-distance transport. This capability allows TP aerosols to modify atmospheric concentration and cloud properties along their path more readily than those in low-altitude regions, thereby impacting both regional atmospheric environment and global climate (Hu et al., 2024). Thus, in-depth exploration of NPF patterns over the TP is crucial for accurately evaluating TP aerosol impact on the global atmosphere and climate.

Research on NPF in the TP background atmosphere is extensive, leading to a comprehensive understanding of its environmental and climatic effects. For instance, a study at the National Atmospheric Background Monitoring Sub-station on Moshi Daban Mountain (3295 m a.s.l.) in Menyuan, Qinghai Province (Gao et al., 2025), found that NPF events occurred on approximately 80 % of the observation days. These events typically started in the morning, with aerosol particle sizes rapidly growing from approximately 5 nm to 150 nm, exhibiting the characteristic "banana-shape" curve. Intensive measurements at Nam Co station (4730 m a.s.l.) in the central TP (Tang et al., 2023) explored NPF frequency and mechanisms, revealing significant seasonal differences: approximately 15 % in the pre-monsoon season but up to 80 % during the summer monsoon. Comprehensive analysis of the CS, gaseous precursors, and meteorological factors, combined with SO_2 and Volatile Organic Compounds (VOCs) simulations, concluded that organics-involved condensation is the dominant NPF mechanism, with CS and gaseous sulfuric acid having negligible influence. Furthermore, the high NPF frequency during the summer monsoon season may be closely linked to frequent southerly and south-westerly airflow. Focusing on the south-eastern TP (Lai et al., 2024), research investigated NPF jointly driven by anthropogenic and biogenic factors. Using field measurements and a chemical transport model, they found frequent NPF events on clear-sky days during the pre-monsoon season, contributing significantly to CCN concentration. Observations confirmed that Highly Oxygenated Organic Molecules (HOM_s) from monoterpene oxidation participate in the nucleation process in this region. (Liu et al., 2024) further showed that the frequent NPF at high-altitude sites in the south-eastern TP is mainly driven by HOMs, including products from monoterpene, and unexpectedly, sesquiterpenes and diterpenes oxidation. Moreover, anthropogenic NO_x emissions were found to play a crucial regulatory role in particle nucleation. Overall, NPF frequency is high in the TP background atmosphere, and its formation is closely related to temperature, relative humidity, and chemical precursor concentrations.

Aerosols generated by NPF in the TP background atmosphere can contribute up to half of the total atmospheric aerosol number concentration and significantly enhance CCN concentration. A study at the world's highest station, Chacaltaya (Rose et al., 2017), analysed 61 % of NPF events, finding they led to increased CCN number concentration, with the probability

https://doi.org/10.5194/egusphere-2026-1628
Preprint. Discussion started: 29 April 2026

reaching 79 % during the wet season due to faster particle growth. The NPF impact on CCN concentration varies seasonally, causing CCN to increase by a factor of 1.54 and 1.36 in spring and winter, respectively. During the summer monsoon season, at a supersaturation of 1.2 %, aerosol number concentration and CCN concentration surged by a factor of 2 and 0.6, respectively, compared to the pre-monsoon season. Furthermore, considering that small particles formed during NPF may continue to grow to CCN activation size over several days, the potential CCN number during the monsoon season may far exceed instantaneous local measurements (Tang et al., 2023). Comparative observations by Shang et al. (2022) indicated that the NPF contribution to total aerosol and CCN concentrations is more significant in the clean atmosphere than that of the polluted atmosphere.

Despite the extensive work summarized above, our understanding of new-particle formation over the TP remains strongly biased toward remote background sites. The urban TP atmosphere—characterised by markedly stronger primary emissions and elevated concentrations of both SO_2 and NO_x—has, so far, received no systematic exploration of its NPF characteristics, governing mechanisms, or quantitative contribution to CCN. This knowledge gap hampers the accurate representation of aerosol sources in regional climate models and precludes a full assessment of the role of urban NPF over the TP in continental CCN budgets. To fill this gap, we carried out seasonal-scale particle number size distribution (PNSD) measurements in Lhasa (3650 m a.s.l.), a high-altitude urban environment on the Tibetan Plateau, during the pre-monsoon and monsoon seasons. The specific aims are (i) to establish an event classification and to quantify the frequency and intensity of urban NPF, (ii) to elucidate the seasonal differences in precursor–meteorology interactions driving NPF, and (iii) to evaluate the instantaneous and seasonal enhancement of CCN concentrations attributable to newly formed particles at the TP urban environment. The observational methodology is described in Section 2, results and discussions are presented in Section 3, and conclusions together with implications for aerosol–climate interactions are summarized in the last Section.

2 Methods

2.1 Sampling sites

As shown in Fig. 1, the study site is located at Tibet University (TU, 29 °38 ′ N, 91 °10 ′ E; 3650 m a.s.l.) in Lhasa, which lies in the south-central TP. Lhasa serves as the capital of the Tibet Autonomous Region and its political, economic, and cultural hub. As one of the largest urban centers on the TP, it is a typical high-altitude city where aerosols are predominantly driven by local sources, including traffic emissions, residential coal/biomass combustion, construction activities, and dust resuspension (Zhao et al., 2022). The site is situated in a broad river valley surrounded by mountains with elevations up to 5500 m a.s.l. Its climate is strongly influenced by the Asian Summer Monsoon and the East Asian Winter Monsoon, with spring and autumn functioning as transitional seasons between these two climate systems (Li et al., 2025). In situ measurements were conducted during two periods: the monsoon period (9 October–10 November 2024) and the pre-monsoon period (25 March–22 April 2025).

https://doi.org/10.5194/egusphere-2026-1628
Preprint. Discussion started: 29 April 2026

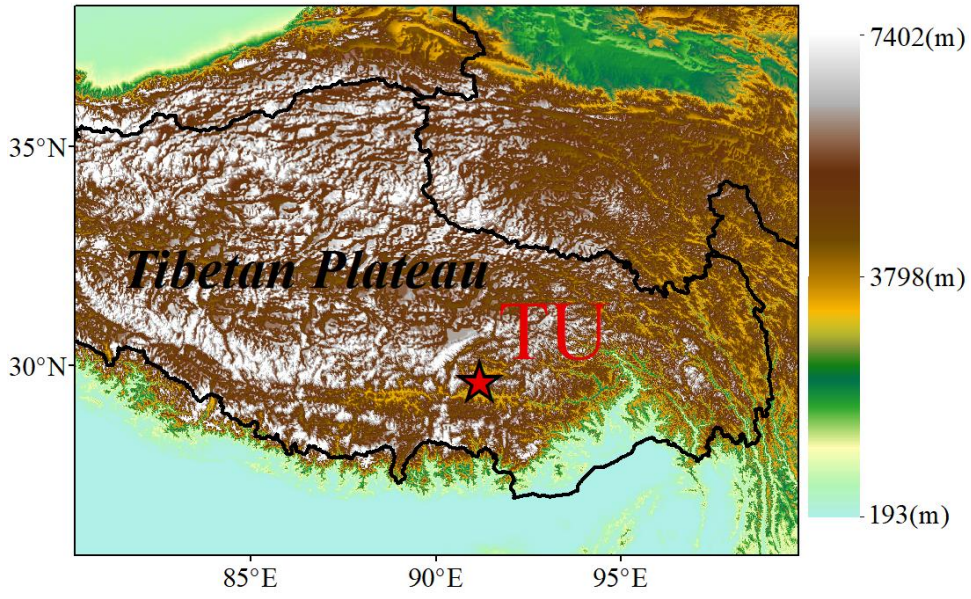

Figure 1: Location and topography of the observation site. Color shading denotes elevation (unit: m).

2.2 Instrumentation

In this study, a comprehensive Scanning Mobility Particle Sizer (SMPS) system was employed to measure the PNSD from 3 to 800 nm with a 5-minute time resolution. This system consisted of two separate instruments from TSI Inc. A nanoparticle SMPS (TSI, Model 3087) was used to measure particles in the size range of 3 to 40 nm, while a standard SMPS (TSI, Model 3080) measured particles from 20 to 800 nm. The two datasets were then merged to create a complete and continuous PNSD. To ensure consistent and accurate measurements, the instruments were housed in a temperature-controlled container maintained at 25 °C. This setup was located on the rooftop of a campus building, with the aerosol inlet positioned approximately 20 meters above ground level. This elevated sampling height was chosen to minimize the influence of localized ground-level emission sources like traffic exhaust and suspended road dust. Furthermore, a silicon diffusion dryer was placed upstream of the SMPSs to reduce the relative humidity of the sampled air to below 40 %, preventing particle growth from water vapour condensation. Ambient aerosols were sampled through a short, conductive tube with minimal bends to reduce size-dependent diffusion losses. All SMPS data underwent rigorous corrections for these diffusion losses and for multiple charging effects to ensure the reliability of the measured particle number concentrations. We also utilized meteorological data from an on-site automatic weather station, which provided essential parameters including temperature (T), relative humidity (RH), wind speed (WS), wind direction (WD), Sulfur Dioxide (SO_2), Nitrogen Dioxide (NO_2), and Ozone (O_3) for a comprehensive analysis of the atmospheric conditions.

https://doi.org/10.5194/egusphere-2026-1628
Preprint. Discussion started: 29 April 2026

2.3 Calculation of variables characterizing new particle formation

The Condensation Sink (CS, unit: s^{-1}) is utilized in this study as a core parameter to quantify the regulating effect of pre-existing aerosols on condensable vapors (Kerminen et al., 2018; Wu et al., 2021). Its calculation is based on the kinetic theory of dilute gases and assumes sulfuric acid (H_2SO_4) as the characteristic condensable substance (Dal Maso, 2005). The calculation process utilizes measured PNSD data and incorporates the influence of ambient temperature (T) and pressure (P). First, the diffusion coefficient of sulfuric acid vapor in the air ($D_{x,\,air}$) is calculated using an empirical formula based on T and P. Subsequently, the mean free path of the condensable vapor (λ) is calculated using the molar mass of sulfuric acid (M_x = 98.08 g/mol). Based on λ and the size-resolved particle radius (R_i), the Knudsen number ($Kn_i = \lambda/R_i$) is determined. To correct the condensation rate from the continuous regime to the transition and free molecular regimes, the transition regime correction factor (β) is introduced (Dinoi et al., 2021):

$$\beta = \frac{Kn+1}{0.377Kn+1+\frac{4}{3\alpha}(Kn^2+Kn)} \quad (1)$$

Here, the sticking coefficient (α) is set to 1.0. Finally, the size-resolved condensation sink (CSi) is determined by $4\pi \cdot Dx,air \cdot Ri \cdot \beta i \cdot ni$, and the total CS value is quantitatively calculated by numerically integrating CSi over all particle size ranges.

$$CS = 2\pi D\int_0^\infty d_p\beta_m(d_p)\times n(d_p)\ \mathrm{d}d_p = 2\pi D\sum_i \beta_i d_{pi}N_i \quad (2)$$

The Coagulation Sink (CoagS, unit: s^{-1}) is another key parameter in atmospheric aerosol dynamics, quantifying the efficiency of pre-existing particles (scavenger particles) in removing specific size-range target particles from the system via the coagulation mechanism (Kulmala et al., 2001). Similar to CS, CoagS is calculated through PNSD integration.

$$CoagS_{d_p} = \int K(d_p,d_p)n(d_p)\mathrm{d}d_p \cong \sum_{d_{p'}=d_p}^{d_{p'}=\max} K(d_p,d_p)N_{d_{p'}} \quad (3)$$

GR, defined as the rate at which the geometric mean diameter of nucleation mode particles increases from dp1 to dp2, was calculated using the procedure outlined by (Kulmala et al., 2012).

$$GR = \frac{\Delta d_p}{\Delta t} = \frac{d_{p2}-d_{p1}}{t_2-t_1} \quad (4)$$

To quantify the intensity of NPF events, we calculated the particle formation rate J (i.e., the rate of aerosol particle formation at a specific size) following the method described by (Baalbaki et al., 2021), which is derived from rearranging the equation governing the time evolution of particle number concentration (Kulmala et al., 2012). Specifically, J was computed for two size bins (dp): 3 nm (J_3), and 7 nm (J_7), with the upper size limits of the corresponding bins set to 7 nm and 20 nm, respectively. The growth rate term in the equation (Eq. 5) was defined as the average of GR measurements for total particles; this GR value was assumed constant during NPF events and set to zero outside the event duration or in non-event periods. The formation rate Jdp is expressed as:

https://doi.org/10.5194/egusphere-2026-1628
Preprint. Discussion started: 29 April 2026

$$J_{d_p} = \frac{dN_{d_p}}{dt} + CoagS_{d_p} \cdot N_{d_p} + \frac{GR}{\Delta d_p} \cdot N_{d_p} \quad (5)$$

CCN concentration is quantitatively calculated based on κ-Köhler theory (Petters and Kreidenweis, 2007). This method aims to determine the number of particles that can be activated at a specific supersaturation (S).

$$A = \frac{4\sigma_{s/a} M_w}{RT\rho_w} \quad (6)$$

$$\kappa = \frac{4A^3}{27 D_c^3 \ln^2 S_c} \quad (7)$$

2.4 NPF Event Classification

In this study, atmospheric particles were divided into three diameter modes: the Nucleation Mode (< 25 nm), the Aitken Mode (25–100 nm), and the Accumulation Mode (> 100 nm) (Wang et al., 2022; Hussein et al., 2020; Kalkavouras et al., 2021; Shen et al., 2022). Event classification was based on the methodology described by Dal Maso (Dal Maso, 2005), which has been widely applied in previous studies of NPF(Gao et al., 2025; Cramer et al., 2026; Lampilahti et al., 2025; Casans et al., 2025). Through visual inspection of the PNSD, the observation days were categorized into four event types. Specifically, NPF days were divided into two main categories: Class I days and Class II days. These types include Class I days (clear and persistent strong events), Class II days (clear but discontinuous moderate events), Undefined days (weak or incomplete NPF characteristics), and Non-Event days (no observable particle formation or growth). Fig. S1–4 presents the daily PNSD for different event types.

Fig. 2a illustrates typical examples of the diurnal evolution of the NPF event categories. On Class I days, the 3 nm particle number concentration began to increase strongly around 09:00, and the mode diameter steadily grew from the Nucleation Mode to the Aitken Mode, persisting until 0:00, displaying the classic "banana shape". On Class II days, the number concentration also began to increase around 09:00, but the growth of the mode diameter only lasted for a few hours, peaking around 13:00. On Undefined days, although an increase in the number concentration of the Nucleation Mode was observed in the morning, the mode diameter remained in the Nucleation Mode between 09:00 and 13:00 without significant growth. On Non-Event days, neither an increase in Nucleation Mode number concentration nor growth into the Aitken Mode was observed. Figure 2c presents a stacked percentage bar chart that quantifies the relative number contributions of nucleation, Aitken, and accumulation modes to the total particle number concentration across these four classified NPF event types. On Class I days, nucleation mode particles account for 42 % of the total number concentration, while Aitken mode particles dominate with a 57 % contribution, and accumulation mode particles contribute a mere 1 %, indicating a scenario where freshly formed nucleation-mode particles undergo rapid growth into the Aitken mode. For Class II days, the nucleation mode overwhelmingly dominates, representing 87 % of the total particle number, with Aitken and accumulation modes contributing only 11 % and 2 %, respectively, which reflects relatively inefficient particle growth after initial formation.

https://doi.org/10.5194/egusphere-2026-1628
Preprint. Discussion started: 29 April 2026

Undefined days exhibit a similar modal contribution pattern to Class II days, with nucleation mode accounting for 78 %, Aitken mode for 19 %, and accumulation mode for 3 %, suggesting some uncertainty in the particle growth process. In contrast, Non-Event days show a more balanced contribution from the three modes, with nucleation mode at 12 %, Aitken mode at 56 %, and accumulation mode at 32 %, reflecting the steady-state particle size distribution of the background atmosphere in the absence of active NPF events. Collectively, this chart highlights the distinct modal contribution characteristics of different NPF event types, providing critical statistical insights into the atmospheric physicochemical processes governing new particle formation and growth.

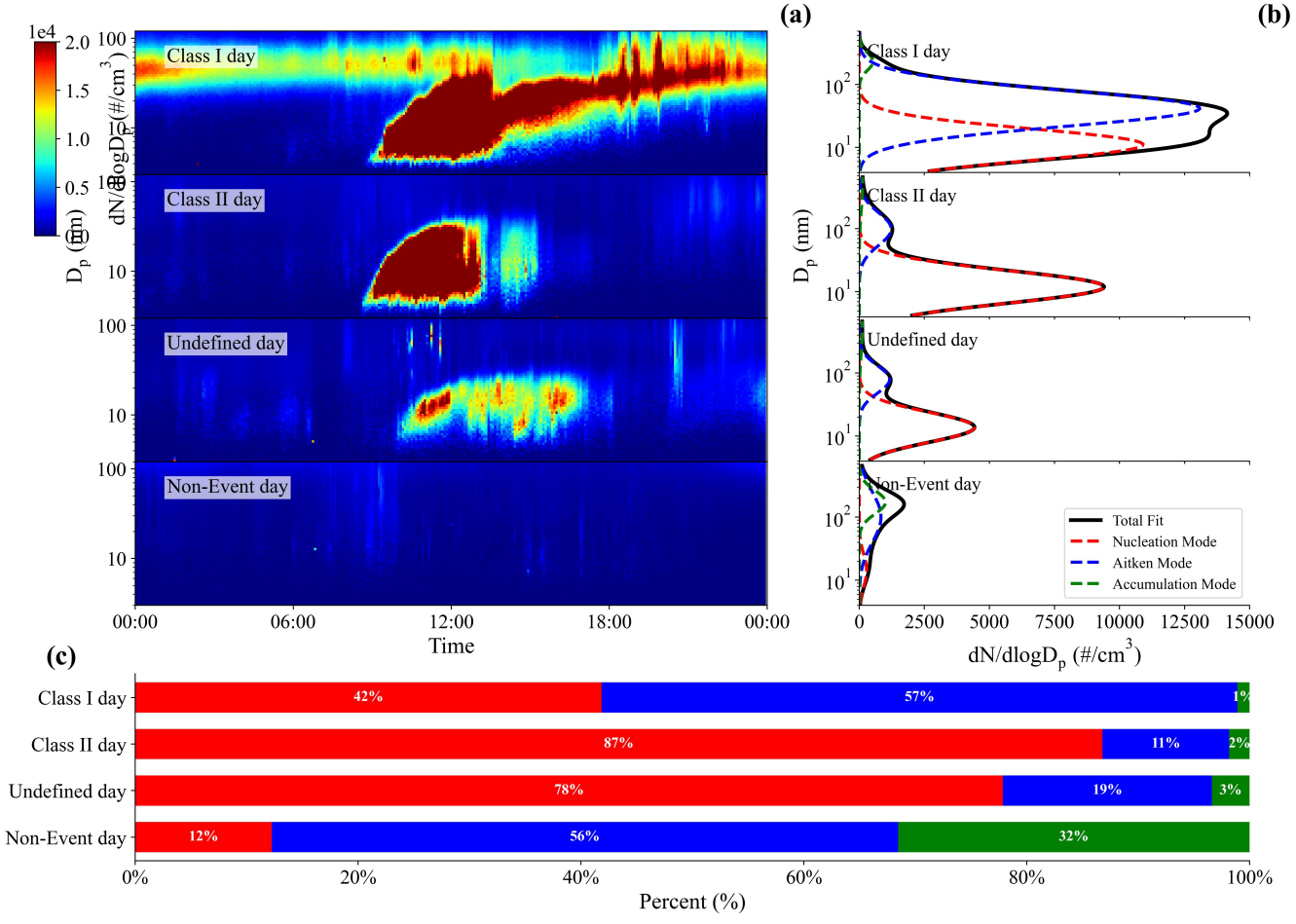

Figure 2: (a) Particle number size distribution evolution, (b) averaged modal fitting, and (c) relative number contributions for four classified NPF event types.

https://doi.org/10.5194/egusphere-2026-1628
Preprint. Discussion started: 29 April 2026

3 Results and discussion

3.1 Overview of the field observations

Meteorological conditions and gaseous pollutants exhibited strong short-term fluctuations and clear diurnal variability during both measurement periods. As shown in Fig. 3a–b, wind speed/wind direction and RH varied substantially on synoptic and diurnal timescales. The monsoon period was characterized by higher RH (41.60 ± 17.78 %) than the pre-monsoon period (27.46 ± 18.23 %). Wind speeds were comparable between the two periods (1.57 ± 0.92 m s^{-1} in the monsoon period and 1.87 ± 1.07 m s^{-1} in the pre-monsoon period), indicating predominantly low-to-moderate ventilation conditions that may facilitate episodic accumulation of precursors and aerosols. Figure 3c–d presents the temporal evolution of SO_2, CS, O_3, and NO_2. O_3 was generally higher during the pre-monsoon period (52.47 ± 14.11 ppb) than during the monsoon period (37.87 ± 12.75 ppb), suggesting a more oxidizing background in the pre-monsoon period. In contrast, SO_2 and NO_2 showed intermittent spikes in both seasons, implying episodic impacts from transport and/or local emissions. Notably, the CS remained similar across seasons (0.0079 ± 0.0053 s^{-1} in the monsoon period and 0.0081 ± 0.0038 s^{-1} in the pre-monsoon period), indicating that the seasonal contrast in NPF occurrence is unlikely driven solely by differences in the pre-existing particle sink.

NPF events were frequently observed at the TU site and were associated with pronounced seasonal differences in PNSD and estimated CCN concentrations. In total, 41 NPF events were identified during the two measurement periods, including 21 Class I event days and 20 Class II event days, in addition to 10 undefined days and 7 non-event days. Based on Fig. 3g, NPF occurrence displayed a marked seasonal contrast, with NPF observed on 86.2 % of the measurement days during the monsoon period but only on 55.1 % during the pre-monsoon period. Consistent with this contrast, Fig. 3e shows that the monsoon period exhibited a substantially higher total particle number concentration ($N_{3–700}$ = 10541 ± 9771 cm^{-3}) than the pre-monsoon period (5335 ± 6886 cm^{-3}), while the median particle diameter (median Dp) was smaller in the monsoon period (36.55 ± 13.99 nm) than in the pre-monsoon period (45.38 ± 33.60 nm), indicating a stronger contribution from smaller particles during the monsoon period. Figure 3f further presents the estimated CCN concentrations and the fractional contributions from different modes. CCN levels were higher during the monsoon period (2812.99 ± 1665.10 cm^{-3}), accompanied by more frequent and more persistent enhancements in the nucleation- and Aitken-mode fractions and episodic reductions in the accumulation-mode fraction, suggesting a shift of the particle population toward the small-to-intermediate size range. In contrast, the pre-monsoon period showed lower CCN (1152.05 ± 608.91 cm^{-3}), weaker and less persistent increases in the nucleation- and Aitken-mode fractions, and a more dominant background contribution from the accumulation mode. Together, these observations highlight strong seasonal modulation of particle sources and CCN-relevant size structure at the TU site and provide context for the process-based analysis in the following sections.

https://doi.org/10.5194/egusphere-2026-1628
Preprint. Discussion started: 29 April 2026

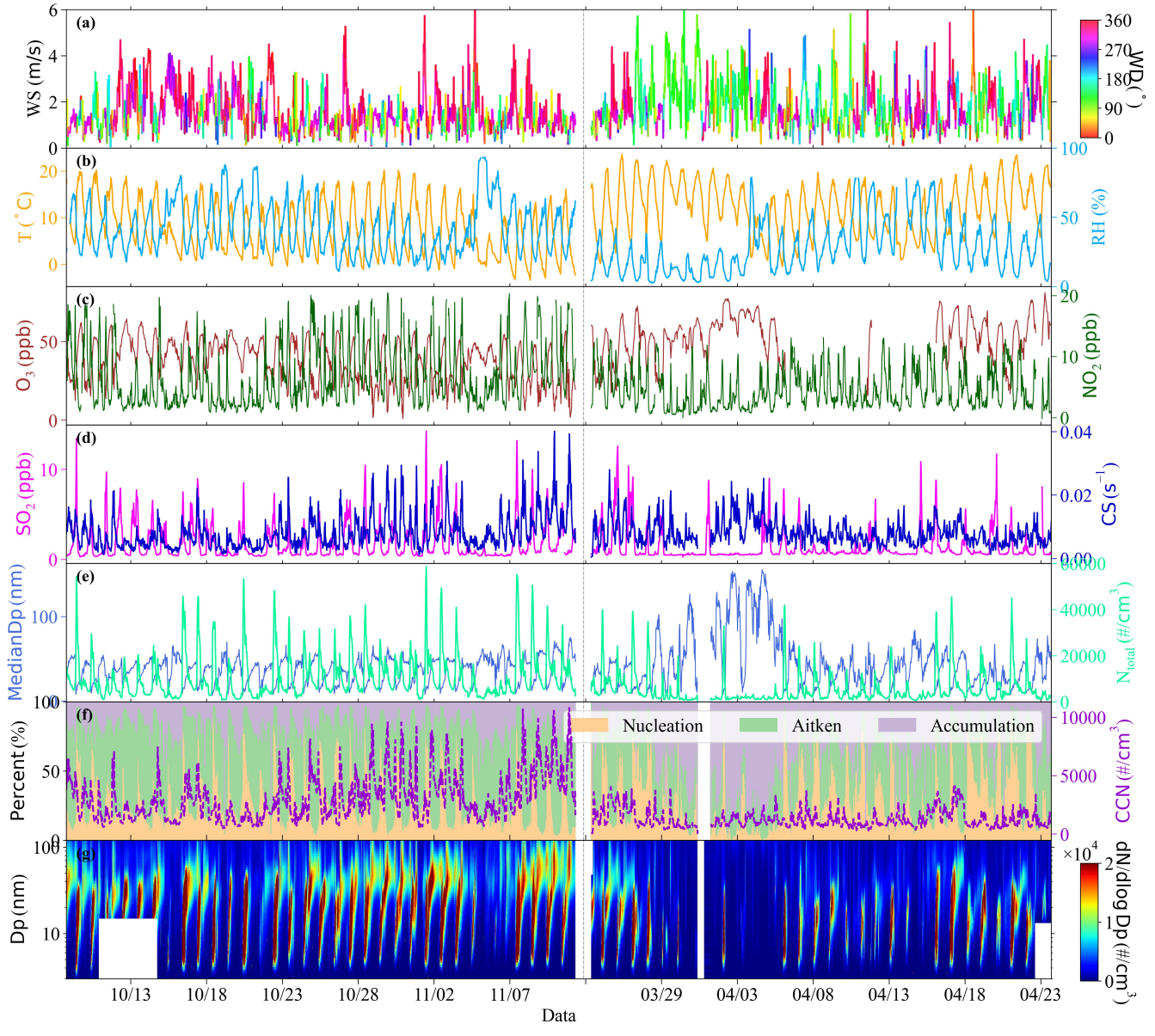

Figure 3: Time series of (a) wind speed and wind direction, (b) ambient temperature and relative humidity, (c) O_3 concentration and NO_2 concentration, (d) SO_2 concentration and Condensation Sink, (e) median particle diameter and particle number concentration in the size range of 3–700 nm, (f) CCN concentration and percentage contributions of the nucleation mode, Aitken mode, and accumulation mode, (g) PNSD during the pre-monsoon and monsoon periods.

https://doi.org/10.5194/egusphere-2026-1628
Preprint. Discussion started: 29 April 2026

3.2 PNSD and number concentration responses

3.2.1 Seasonal mean PNSD and modal contributions

Seasonal mean PNSD and modal contributions reveal a distinct background size structure and surface/volume partitioning between the monsoon and pre-monsoon periods. Figure 4a shows that the seasonal mean PNSD at the TU site is typically multimodal, reflecting the combined influences of secondary particle production, growth, and the pre-existing aerosol population. A pronounced seasonal contrast is evident in the total number concentration: the mean $N_{3–700}$ during the monsoon period (10541 ± 9771 # cm^{-3}) was 1.98 times higher than that during the pre-monsoon period (5335 ± 6886 # cm^{-3}) (Fig. 4a). In terms of modal partitioning, Fig. 4b indicates that while the Aitken mode dominates number concentration in both periods, the surface area and volume are strongly controlled by the accumulation mode in the pre-monsoon period, accounting for 85 % (surface area) and 96 % (volume). In contrast, during the monsoon period the Aitken mode contributes substantially more to surface area (42 %) and volume (25 %) than in the pre-monsoon period (14 % and 4 %, respectively), consistent with a particle population shifted toward smaller-to-intermediate sizes. These seasonal differences provide a baseline for interpreting event-day diurnal changes and their implications for CCN-relevant size fractions.

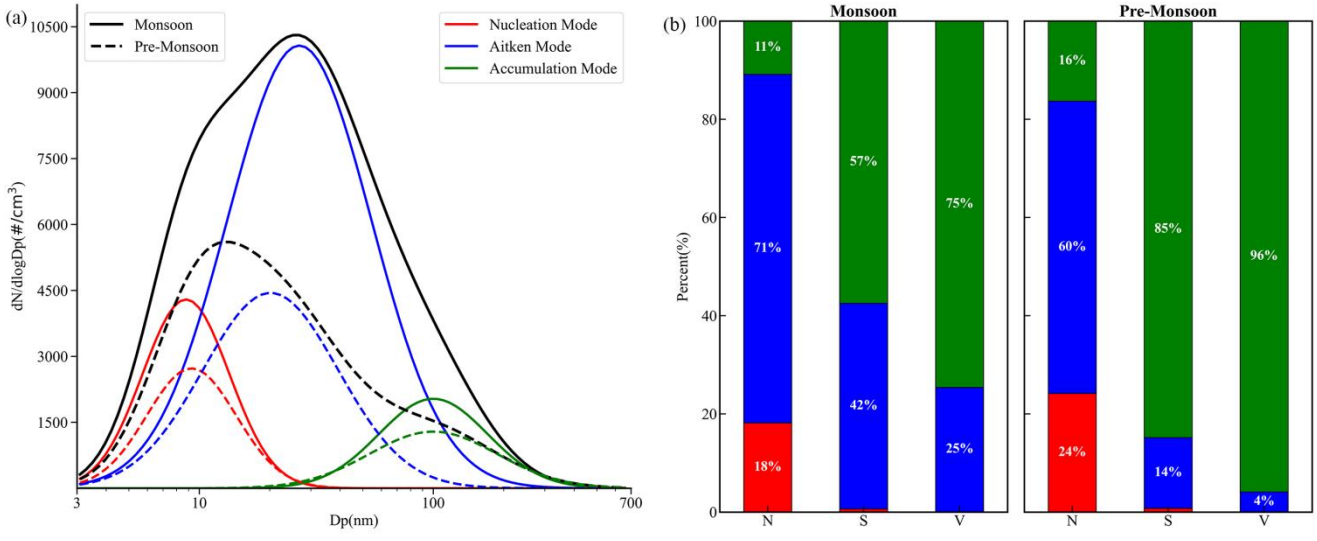

Figure 4: (a) Particle number size distribution characteristics and (b) modal contributions to number (N), surface area (S), and volume (V) distributions during monsoon and pre-monsoon periods.

3.2.2 Diurnal variations of size-segregated number concentrations

Event-day diurnal profiles show a clear sequence from daytime ultrafine particle production to enhanced Aitken-mode concentrations, whereas non-event days exhibit weaker and less structured variability. Figure 5 summarizes diurnal profiles of particle number concentrations for the nucleation ($N_{3–25}$), Aitken ($N_{25–100}$), accumulation ($N_{100–700}$), and total ($N_{3–700}$) size

https://doi.org/10.5194/egusphere-2026-1628
Preprint. Discussion started: 29 April 2026

ranges across different day types. The nucleation-mode number concentration exhibits a sharp, transient noon-time maximum (12:00 local time) across all categories, followed by a rapid decline (Fig. 5a). In contrast, the Aitken mode displays strong category dependence: Class I days show a pronounced bimodal pattern with a primary peak around 12:00 and a secondary peak around 19:00 (with a weaker perturbation near 15:00), whereas Class II, Undefined, and Non-Event days are largely unimodal with a single noon-time peak (Fig. 5c). The accumulation mode follows a similar but weaker pattern (Fig. 5d), and the total number concentration mirrors the nucleation-mode noon peak while retaining a distinct evening enhancement on Class I days, consistent with sustained growth and modal evolution into the Aitken range (Fig. 5b). These diurnal statistics indicate that the impact of NPF on the size distribution depends not only on daytime particle production, but also on the persistence of growth into the Aitken mode.

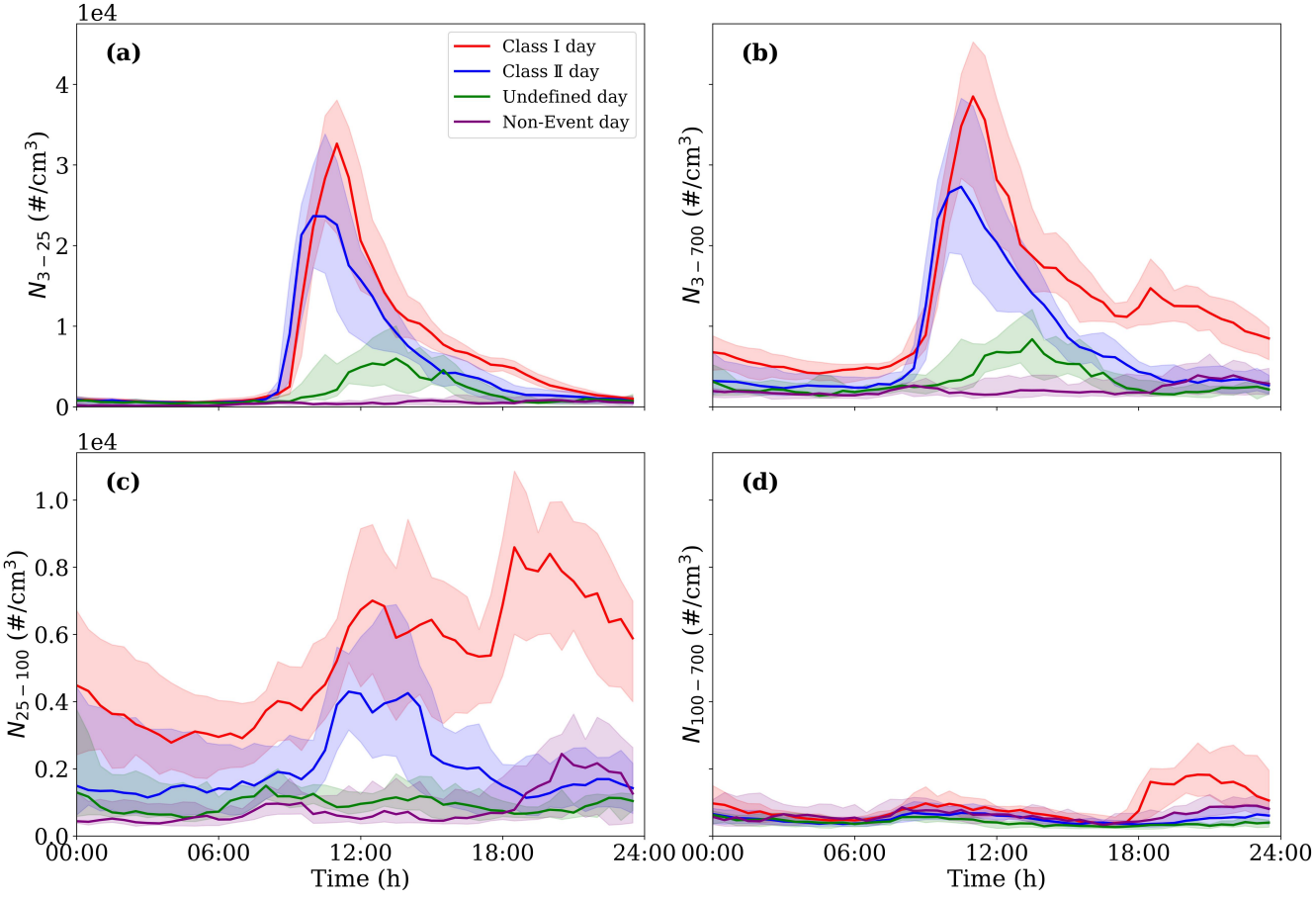

Figure 5: Diurnal variation of aerosol number concentrations (# cm^{-3}) at the size ranges of (a) 3–25 nm, (b) 3–700 nm, (c) 25–100 nm, and (d) 100 – 700 nm, during Class I day, Class II day, Undefined day, and Non-Event day. Shaded areas represent the interquartile range (25th to 75th percentiles).

https://doi.org/10.5194/egusphere-2026-1628
Preprint. Discussion started: 29 April 2026

3.3 Factors controlling the formation and development of NPF events

3.3.1 Formation and growth characteristics

The formation and growth characteristics of NPF were quantified using particle formation rates (J) and growth rates (GR), and the diurnal evolution of formation rates in the 3–7 nm and 7–20 nm size ranges is summarized in Fig. 6. On NPF days, both Class I and Class II events exhibit pronounced daytime increases in (J_{3-7}), consistent with active photochemically driven particle production during the morning to midday period, whereas Non-Event days show substantially weaker formation. Averaged over the daytime period (08:00–16:59), the mean formation rates in the initial nucleation stage (3–7 nm) were 1.13 ± 1.60 cm^{-3} s^{-1} for Class I events and 1.15 ± 1.69 cm^{-3} s^{-1} for Class II events, indicating strong daytime particle production for both event classes. These values are close to results from the Nam Co station (J_4: 1.15 ± 0.58 cm^{-3} s^{-1}) (Tang et al., 2023) and the Mt. Yulong station (J_3: 1.18 cm^{-3} s^{-1}) (Shang et al., 2018). As particles evolved into the 7–20 nm range, the formation rate (J_{7-20}) further intensified to approximately 3.6 cm^{-3} s^{-1}, remaining within the reasonable range established by high-altitude environmental observations. Regarding growth kinetics, the observed GR_{3-7} (2.31–3.16 nm h^{-1}) and GR_{7-20} (2.97 – 3.51 nm h^{-1}) were comparable to values at Nam Co (GR_{4-25}: 4.0 ± 1.2 nm h^{-1}) and Mt. Yulong (3.2 nm h^{-1}), significantly exceeding those at the NCO-P station (1.18 ± 0.7 nm h^{-1}) (Venzac et al., 2008) and Mt. Daban (2.0 nm h^{-1}) (Du et al., 2015). In summary, the J and GR values at TU are well within the ranges reported for global high-altitude environments, indicating that the site experiences characteristic high-altitude NPF with strong daytime formation and sufficiently rapid growth to promote downstream enhancement of Aitken-mode number concentrations.

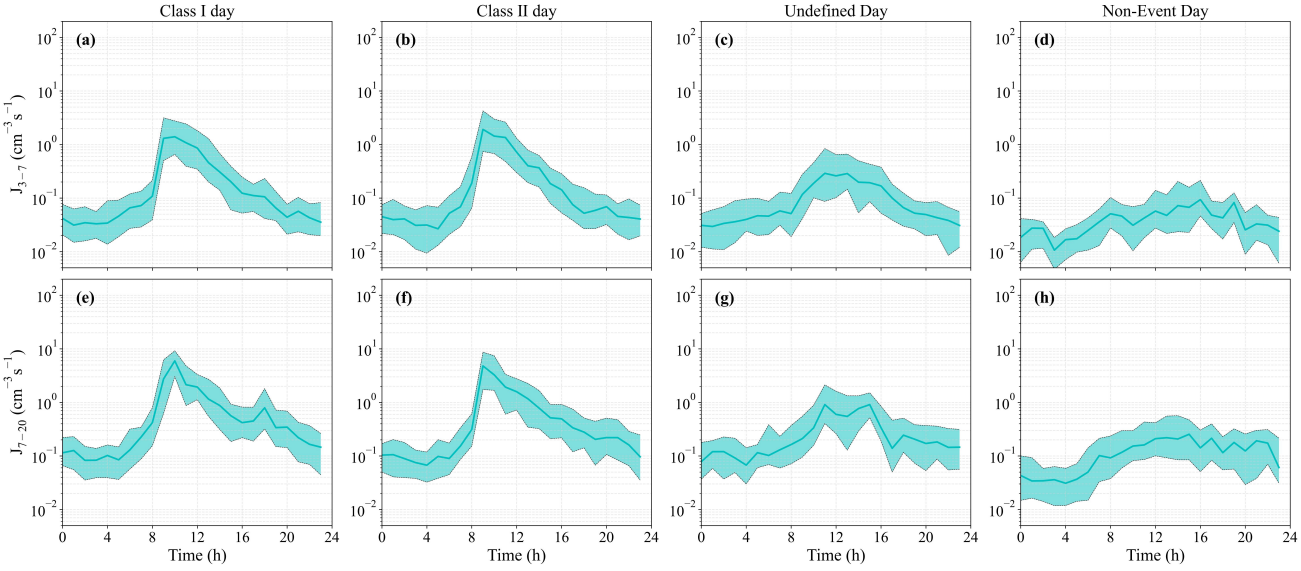

Figure 6: Diurnal variations of the formation rates J3 during (a) Class I day, (b) Class II day, (c) Undefined day, and (d) Non-Event day periods. The corresponding diurnal variations of the formation rate J_7 were shown in panels (e), (f), (g), and (h). The shaded areas represent the 25th and 75th percentile boundaries, and the solid lines denote the median values.

https://doi.org/10.5194/egusphere-2026-1628
Preprint. Discussion started: 29 April 2026

3.3.2 Condensation sink and its role

CS represents the ability of the pre-existing aerosol population to remove condensable vapors via condensation, while CoagS describes the loss of freshly formed clusters and ultrafine particles through collision and coalescence with larger background particles (Victor et al., 2024). Figure 7 shows the diurnal variations of CS and CoagS for different day types and seasons. Both sink terms exhibit clear diurnal structure and substantial variability, indicating that the removal capacity for vapors and nascent particles can change markedly over the course of a day and between different regimes.

Consistent with many studies reporting that NPF tends to be favored under relatively low CS (Cai et al., 2017; Saha et al., 2018; Kalivitis et al., 2019; Kalkavouras et al., 2020; Aktypis et al., 2023), the TU site nevertheless shows that NPF can occur even when CS is not minimal. The mean CS levels (±1σ) are 0.0079 ± 0.0044 s^{-1} for Class I days, 0.0060 ± 0.0042 s^{-1} for Class II days, 0.0053 ± 0.0045 s^{-1} for Undefined days, and 0.0064 ± 0.0044 s^{-1} for Non-Event days (Fig. 7 a–d). Thus, CS on NPF days is slightly higher than that on Non-Event days, and the NPF-day mean CS at TU is higher than values reported for remote plateau background sites in China (Tang et al., 2023), yet lower than those reported for the major urban environment of Beijing (Du et al., 2017), suggesting an intermediate sink environment characteristic of a high-altitude urban setting. Importantly, despite the strong seasonal contrast in NPF frequency, seasonal mean CS is broadly similar between the monsoon (0.0069 ± 0.0041 s^{-1}) and pre-monsoon (0.0062 ± 0.0047 s^{-1}) periods (Fig. 7e–f), indicating that differences in the pre-existing particle sink are unlikely to be the primary driver of the seasonal contrast in NPF occurrence.

In contrast, CoagS shows a stronger separation among day types and seasons. The mean CoagS values are $5.27 \times 10^{-11} \pm 2.62 \times 10^{-11}$ s^{-1} for Class I days, $3.66 \times 10^{-11} \pm 2.39 \times 10^{-11}$ s^{-1} for Class II days, $2.57 \times 10^{-11} \pm 1.53 \times 10^{-11}$ s^{-1} for Undefined days, and $2.55 \times 10^{-11} \pm 1.41 \times 10^{-11}$ s^{-1} for Non-Event days. Seasonally, CoagS is also markedly higher during the monsoon ($4.85 \times 10^{-11} \pm 2.57 \times 10^{-11}$ s^{-1}) than during the pre-monsoon period ($2.88 \times 10^{-11} \pm 1.93 \times 10^{-11}$ s^{-1}). Since CoagS directly reflects the scavenging loss of freshly formed clusters, the elevated monsoon CoagS suggests a stronger survival constraint on nascent particles. However, this constraint did not prevent the higher NPF frequency observed during the monsoon period, implying that enhanced precursor availability and favorable photochemical conditions likely outweighed the increased coagulation loss.

Taken together, these results suggest that the occurrence and development of NPF at TU is better interpreted as a competition between source processes and sink processes, rather than being controlled by sink alone. This interpretation is consistent with previous observations that NPF can be observed under moderate sinks when vapor production is sufficiently strong (Zhang et al., 2021; Sellegri et al., 2019; Wang et al., 2022; Baalbaki et al., 2021). In this framework, CoagS provides an additional constraint on whether newly formed clusters can survive long enough to grow into larger sizes, while CS limits the availability of low-volatility vapors required for sustained growth; hence, event intensity and downstream impacts are expected to depend on the joint evolution of formation/growth rates and sinks over the diurnal cycle.

https://doi.org/10.5194/egusphere-2026-1628
Preprint. Discussion started: 29 April 2026

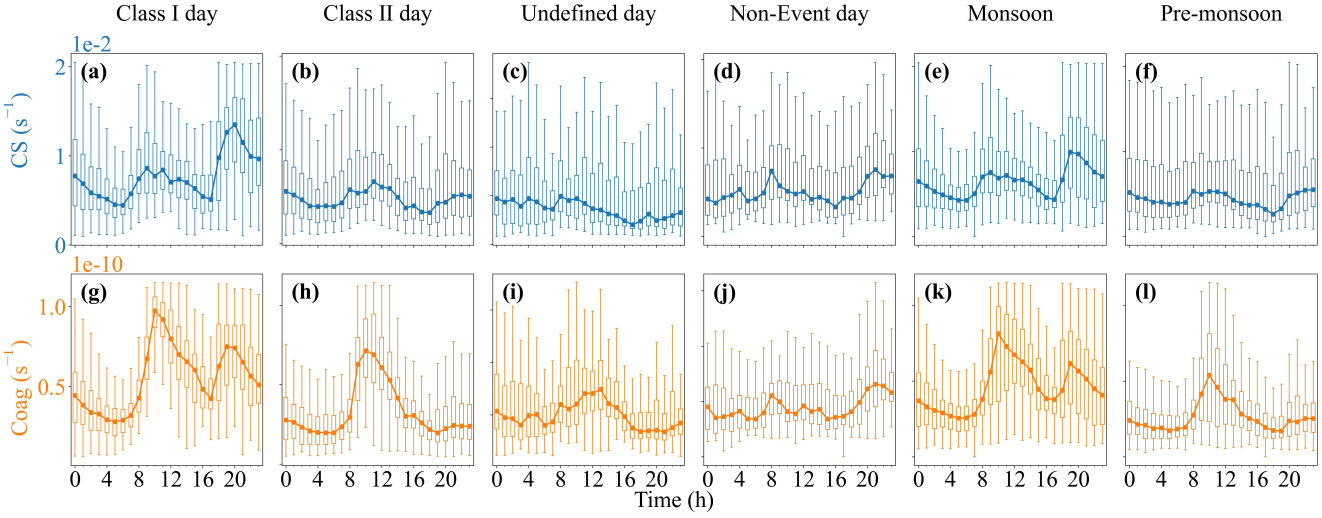

Figure 7: Diurnal variations of condensation sink and coagulation sink for different event classifications and seasons.

3.3.3 Meteorology and precursor modulation, with transport context

Meteorological conditions during the study period show clear diurnal variability in temperature and relative humidity, consistent with the strong dependence of NPF on atmospheric state and precursor availability reported in previous studies (Hakala et al., 2022; Kalkavouras et al., 2020; Kalkavouras et al., 2019; Victor et al., 2024; Singh et al., 2025). The site was predominantly under clear to partly cloudy conditions with sufficient solar radiation, occasionally interrupted by precipitation. Notably, an extended rainfall episode occurred from 4 to 6 November during the monsoon period, during which no NPF events were identified. This is consistent with wet scavenging and suppressed photochemical production of condensable vapors during precipitation, both of which reduce particle number concentrations and interrupt the NPF process. To quantify how meteorology and key gaseous precursors are associated with NPF, we compared SO_2, O_3, and NO_2 together with temperature, RH, and wind speed across day types and seasonal backgrounds. Marked seasonal contrasts were observed: mean temperature was higher in the pre-monsoon period (11.38 ± 5.77 °C) than in the monsoon period (7.77 ± 5.60 °C), whereas RH was substantially higher in the monsoon (42.02 ± 18.11 %) than in the pre-monsoon period (28.57 ± 20.42 %). Wind speed was slightly higher in the pre-monsoon period (2.46 ± 1.78 m s^{-1}) than in the monsoon period (1.97 ± 1.32 m s^{-1}), implying comparatively weaker ventilation during the monsoon that may favor episodic accumulation of precursors and vapors.

During the monsoon season, NPF days exhibited substantially higher SO_2 and NO_2 than non-NPF days: SO_2 averaged 1.92 ± 2.08 ppb on NPF days, clearly exceeding 0.73 ± 0.75 ppb on non-NPF days, while NO_2 averaged 7.74 ± 5.69 ppb on NPF days compared with 4.38 ± 2.99 ppb on non-NPF days. The sector plots further indicate that elevated SO_2 and NO_2 occur more frequently under southerly transport on NPF days, whereas concentrations in the corresponding sectors are generally lower on non-NPF days (Fig. 8). Because SO_2 oxidation by OH· produces H_2SO_4, and H_2SO_4 is widely recognized as a key

https://doi.org/10.5194/egusphere-2026-1628
Preprint. Discussion started: 29 April 2026

nucleation precursor and critical for early particle growth, monsoon-season NPF at the site can be interpreted as a precursor-driven process in which SO_2 plays a central role (Olin et al., 2020; Yao et al., 2018; Kerminen et al., 2018). Although elevated NO_2 may suppress $OH\cdot$ and O_3 production by promoting radical termination and thereby hinder nucleation, the clearly elevated SO_2 observed on NPF days suggests that plentiful SO_2 increases the potential for H_2SO_4 formation. This interpretation is further supported by Fig. S5, which shows that during the particle-formation period SO_2 concentrations on NPF days are clearly higher than those on non-NPF days, suggesting that the promoting effect of SO_2 may outweigh the inhibitory effect associated with elevated NO_2. This may partly offset NO_x-related suppression and enable NPF events to occur (Gao et al., 2025).

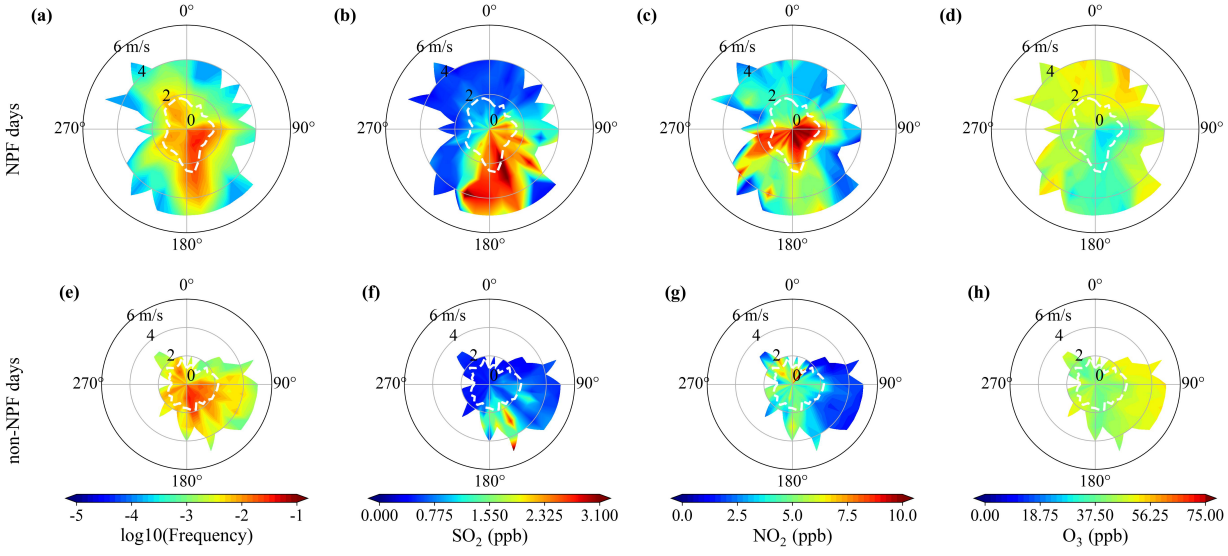

Figure 8: Wind-sector analysis comparing the distributions of (a) wind speed and wind direction frequency together with sector-averaged concentrations of (b) SO_2, (c) NO_2, and (d) O_3, for NPF days during the monsoon period; panels (e), (f), (g), and (h) show the corresponding wind-sector frequency and gas concentrations for non-NPF days during the monsoon period.

During the pre-monsoon period, NPF formation is influenced by multiple factors and does not exhibit a single, well-defined controlling pattern. As shown in Figs. 9 and S6, although SO_2, NO_2, and O_3 differ to some extent between NPF and non-NPF days, the overall separation remains limited, while wind speed and wind direction also fail to show a consistent or distinctive signal. These results suggest that pre-monsoon NPF is more likely governed by the combined effects of multiple factors, including precursor supply, atmospheric oxidation, and boundary-layer evolution, rather than by any single dominant factor (Wu et al., 2024). Given that the contrast in inorganic gaseous precursors is generally weak, the possible contribution of VOC-related oxidation processes to the initial growth of newly formed particles deserves attention (Zhang et al., 2026; Yang et al., 2026). However, because direct observations of VOCs and their oxidation products are not available in this study, their specific role cannot be further constrained and still requires additional investigation.

https://doi.org/10.5194/egusphere-2026-1628
Preprint. Discussion started: 29 April 2026

Overall, the seasonal comparison highlights a clear seasonality in the controlling factors of NPF. During the monsoon season, NPF appears primarily driven by SO_2 availability and its oxidation to H_2SO_4, consistent with a "sulfur-precursor-limited" regime; although elevated NO_2 may exert inhibitory effects through radical termination, this suppression may be partly compensated by the higher acid formation potential under high SO_2. In contrast, during the pre-monsoon season, NPF appears to be governed by the combined influence of multiple processes rather than by a single dominant factor, with precursor availability, atmospheric oxidation, and boundary-layer evolution all likely playing a role; the possible contribution of VOC-related oxidation to early particle growth deserves attention but remains to be further constrained.

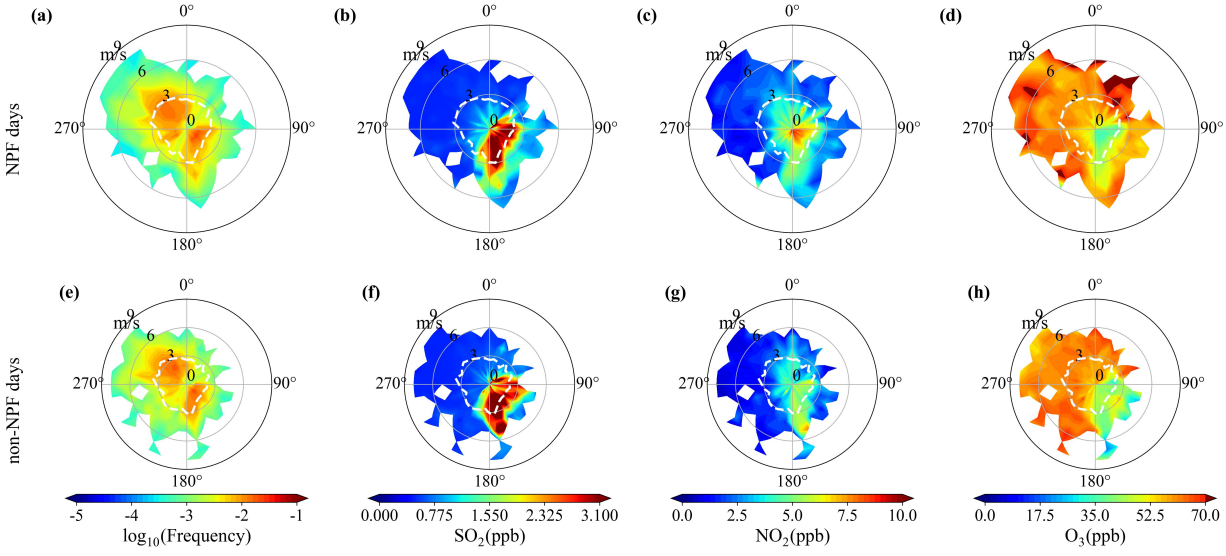

Figure 9: Wind-sector analysis comparing the distributions of (a) wind speed and wind direction frequency together with sector-averaged concentrations of (b) SO_2, (c) NO_2, and (d) O_3, for NPF days during the pre-monsoon period; panels (e), (f), (g), and (h) show the corresponding wind-sector frequency and gas concentrations for non-NPF days during the pre-monsoon period.

3.4 Modulation of CCN by NPF in urban air

To quantify the influence of NPF on CCN in the urban atmosphere of the Tibetan Plateau, we examined both the diurnal evolution and the distribution of CCN for different event categories as well as for the two seasonal periods (monsoon and pre-monsoon). Because direct measurements of CCN concentration were unavailable in this study, CCN was estimated from the measured PNSD using the κ-Köhler framework described in Sect. 2.3, assuming a constant particle hygroscopicity parameter κ of 0.12 and a supersaturation S of 1.2 %.

Fig. 10 illustrates pronounced event-type dependence of CCN in both diurnal evolution and overall distribution. CCN on Class I days remains substantially higher than in all other categories throughout the day and shows a strong late-day enhancement, with the highest values occurring from the late afternoon to evening (Shen et al., 2019). A weaker morning increase is also evident, but the dominant feature is the marked evening rise, consistent with sustained growth and survival of

https://doi.org/10.5194/egusphere-2026-1628
Preprint. Discussion started: 29 April 2026

newly formed particles into CCN-relevant sizes later in the day. In contrast, Class II days exhibit more moderate CCN levels with a broad daytime elevation and a weaker enhancement around midday, whereas Undefined and Non-Event days remain comparatively low and display only weak diurnal variability aside from a modest late-evening increase. The median (IQR) CCN concentration is 1095.3 (750.2–1678.9) cm^{-3} on Non-Event days. By comparison, CCN is highest and most broadly distributed on Class I days, with a median (IQR) of 3032.0 (1823.5–4513.5) cm^{-3} and an extended upper tail, followed by Class II days at 1285.7 (823.4–2066.2) cm^{-3} and Undefined days at 811.5 (610.4–1083.6) cm^{-3}. The average CCN concentration (±1 standard deviation) follows the same ranking: 3351 ± 1919 cm^{-3} (Class I) > 1540.2 ± 872.1 cm^{-3} (Class II) > 1278.1 ± 667.6 cm^{-3} (Non-Event) > 880.5 ± 374.4 cm^{-3} (Undefined). These results further suggest that the CCN influence of NPF depends not only on nucleation occurrence, but also on the persistence of particle growth and survival after formation.

Seasonal perspective. The seasonal distributions show substantially higher CCN during the monsoon period than during the pre-monsoon period (Fig. 10b), consistent with the higher NPF frequency reported in Sect. 3.1. The monsoon median CCN is 2448.9 (1471.5–3820.6) cm^{-3} with a mean of 2813.0 ± 1665.2 cm^{-3}, whereas the pre-monsoon median is 964.7 (696.4–1489.6) cm^{-3} with a mean of 1152.1 ± 608.9 cm^{-3}. This seasonal contrast indicates that enhanced secondary particle production and subsequent growth during the monsoon can maintain a markedly elevated CCN background in this high-altitude urban environment.

Overall, our results demonstrate that NPF is an effective source of CCN in the TP urban atmosphere, but its impact is strongly modulated by event type and season. The pronounced late-day CCN enhancement and the broad, high-CCN distribution on Class I days highlight the importance of sustained post-formation growth and particle survival in determining the strength of the CCN response. At the seasonal scale, the markedly elevated CCN levels during the monsoon indicate that frequent NPF events, together with favorable growth conditions, jointly sustain a high CCN background. This implies that secondary aerosol formation may play a more important role in aerosol–cloud interactions over high-altitude urban regions.

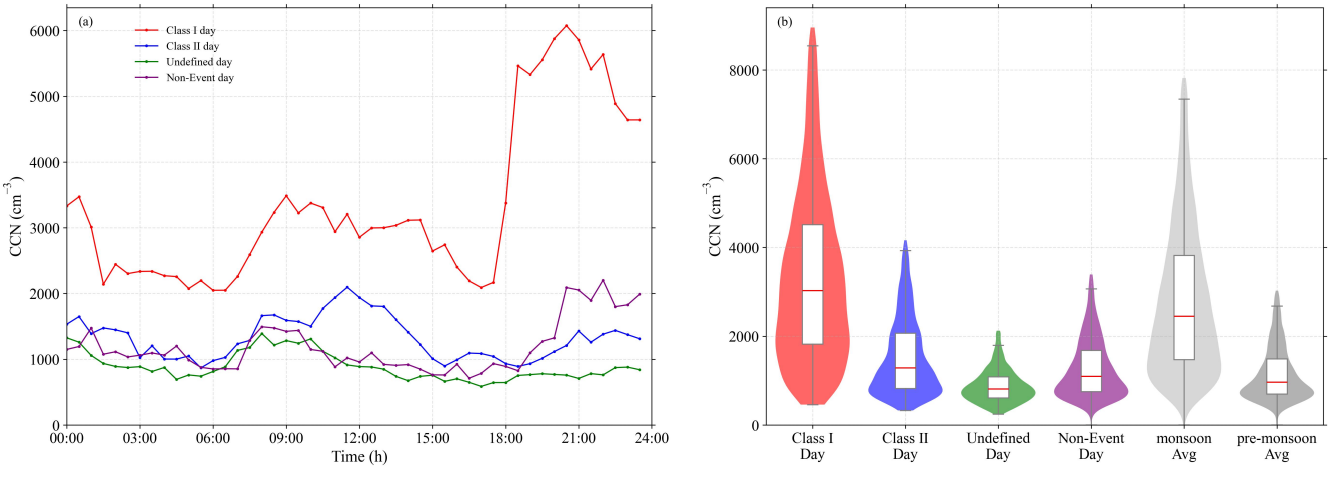

https://doi.org/10.5194/egusphere-2026-1628
Preprint. Discussion started: 29 April 2026

Figure 10: Diurnal variation (a) and statistical distribution (b) of CCN concentration during different days, classified by NPF events.

4 Conclusion

This study provides a comprehensive characterization of NPF in Lhasa, a high-altitude urban center on the Tibetan Plateau, with particular emphasis on the controlling factors of NPF and its implications for CCN during the pre-monsoon and monsoon seasons. Frequent NPF was observed throughout the campaigns. The seasonal contrast in NPF occurrence was pronounced, with event frequencies of 86.2 % in the monsoon and 55.1 % in the pre-monsoon, highlighting that the NPF regime in Lhasa is highly sensitive to seasonally varying meteorology and atmospheric chemistry.

The results indicate that NPF in this high-altitude urban atmosphere is not primarily limited by the pre-existing particle sink, but is more strongly governed by precursor availability and oxidative capacity. The CS remained comparable between seasons, suggesting that the marked seasonal change in NPF frequency cannot be explained by sink suppression alone. Instead, the chemical–meteorological context differs substantially across seasons. During the monsoon, NPF days were associated with elevated SO_2, consistent with intensified sulfur-related photochemical production of condensable vapors under abundant radiation, pointing to a regime where sulfuric-acid-driven nucleation and early growth are favored. In contrast, pre-monsoon NPF did not show a single, well-defined controlling factor, but was more likely influenced by the combined effects of precursor supply, atmospheric oxidation, and boundary-layer evolution. Under such conditions, VOC-related oxidation may contribute to the early growth of newly formed particles, although its specific role remains to be further constrained.

A key outcome of this work is that NPF substantially enhances CCN in Lhasa, and the magnitude of the CCN response is governed by event strength and, critically, by whether newly formed particles can sustain growth after nucleation to reach CCN activation diameters. CCN concentrations followed a clear hierarchy of Class I > Class II > non-event > undefined, indicating that strong NPF events can maintain a markedly elevated CCN population relative to background conditions. The diurnal evolution further shows that the CCN enhancement is most pronounced from late afternoon to evening on Class I days, consistent with a persistent “banana-shaped” growth pattern and efficient survival of freshly formed particles into the size range where they can be activated as CCN. On a seasonal basis, mean CCN during the monsoon exceeded that during the pre-monsoon by more than a factor of two, implying that frequent NPF combined with favorable growth conditions can raise the CCN background level in this high-altitude urban region and potentially influence aerosol–cloud interactions over the TP. Deepening our understanding of NPF over the Tibetan Plateau is essential for more accurately assessing the impacts of aerosols in the TP on the global atmospheric environment and climate, and it can provide a solid scientific basis for the formulation of relevant policies.

Despite the insights gained in this study, several limitations should be acknowledged. First, the classification of NPF events was mainly based on visual inspection of the daily evolution of particle number size distributions and modal development. Although this approach has been widely used in previous studies, some uncertainty may still exist, particularly for weak

https://doi.org/10.5194/egusphere-2026-1628
Preprint. Discussion started: 29 April 2026

events or those with discontinuous growth. Second, CCN concentrations were not directly measured but estimated from the measured PNSD using the κ-Köhler framework, which may introduce uncertainties associated with the assumed hygroscopicity parameter and supersaturation. Therefore, the estimated CCN values are more suitable for interpreting relative differences and response patterns than for over-interpreting their absolute magnitudes. In addition, due to the lack of direct observations of VOCs and their oxidation products, the mechanisms of NPF, especially during the pre-monsoon period, could not be further constrained. Future studies should combine longer-term continuous observations with direct CCN measurements and additional observations of VOCs, H_2SO_4, and related oxidation products, in order to better identify the controlling factors of NPF and its contribution to CCN in high-altitude urban environments over the Tibetan Plateau.

Code and data availability

The elevation data used in this study are openly available from the Geospatial Data Cloud at https://www.gscloud.cn.
The raw observational datasets used in this study have been deposited in Zenodo and can be freely downloaded from https://doi.org/10.5281/zenodo.19876491.
The codes used for data processing and figure generation have been deposited in a separate Zenodo repository and can be freely downloaded from https://doi.org/10.5281/zenodo.19879177.

Author contributions

QM and LW wrote the manuscript. QM, LW, GZ, CY, JS and TZ discussed the original idea and results. JS, FS, TL, YG, and YC conducted the field measurement. QM, LW and JS processed and analysed the data.

Competing interests

The authors declare that they have no conflict of interest.

Financial support

This study was financially supported by the National Natural Science Foundation of China (42405083), the Open Project of the Key Laboratory of Biodiversity and Environment on the Qinghai-Tibet Plateau, Ministry of Education (KLBE2025010), the Tibetan Key Research and Development Program Project (XZ202403ZY0022).

https://doi.org/10.5194/egusphere-2026-1628
Preprint. Discussion started: 29 April 2026

References

Aktypis, A., Kaltsonoudis, C., Skyllakou, K., Matrali, A., Vasilakopoulou, C. N., Florou, K., and Pandis, S. N.: Infrequent new particle formation in a coastal Mediterranean city during the summer, Atmospheric Environment, 302, 119732, https://doi.org/10.1016/j.atmosenv.2023.119732, 2023.

Arias, P., Bellouin, N., Coppola, E., Jones, R., Krinner, G., Marotzke, J., Naik, V., Palmer, M., Plattner, G.-K., and Rogelj, J.: Climate Change 2021: the physical science basis. Contribution of Working Group I to the Sixth Assessment Report of the Intergovernmental Panel on Climate Change; technical summary, 2021.

Baalbaki, R., Pikridas, M., Jokinen, T., Laurila, T., Dada, L., Bezantakos, S., Ahonen, L., Neitola, K., Maisser, A., Bimenyimana, E., Christodoulou, A., Unga, F., Savvides, C., Lehtipalo, K., Kangasluoma, J., Biskos, G., Petäjä, T., Kerminen, V. M., Sciare, J., and Kulmala, M.: Towards understanding the characteristics of new particle formation in the Eastern Mediterranean, Atmos. Chem. Phys., 21, 9223–9251, 10.5194/acp-21-9223-2021, 2021.

Cai, R., Yang, D., Fu, Y., Wang, X., Li, X., Ma, Y., Hao, J., Zheng, J., and Jiang, J.: Aerosol surface area concentration: a governing factor in new particle formation in Beijing, Atmos. Chem. Phys., 17, 12327–12340, 10.5194/acp-17-12327-2017, 2017.

Casans, A., Casquero-Vera, J. A., Rejano, F., Lyamani, H., Cazorla, A., Zabala, I., Huang, W., Agro, M., Barreto, A., Rodriguez, S., Gonzalez, Y., Bianchi, F., Petaja, T., Olmo, F. J., Alados-Arboledas, L., Carinanos, P., Gysel-Beer, M., and Titos, G.: Determining the impact of new particle formation events on cloud condensation nuclei (CCN) concentrations, Sci Total Environ, 972, 179094, 10.1016/j.scitotenv.2025.179094, 2025.

Cramer, K. L., Guenther, A. B., and Smith, J. N.: Ultrafine aerosol formation and growth in a Southern California desert, Aerosol Science and Technology, 1–13, 10.1080/02786826.2026.2619538, 2026.

Dal Maso, M., Kulmala, M., Riipinen, I., Wagner, R., Hussein, T.,Aalto, P. P., and Lehtinen, K. E.: Formation and growth of fresh atmospheric aerosols: eight years of aerosol size distribution data from SMEAR II, Hyytiälä, Finland, Boreal environment research, 10, 323, 2005.

Dinoi, A., Weinhold, K., Wiedensohler, A., and Contini, D.: Study of new particle formation events in southern Italy, Atmospheric Environment, 244, 117920, https://doi.org/10.1016/j.atmosenv.2020.117920, 2021.

Du, W., Sun, Y. L., Xu, Y. S., Jiang, Q., Wang, Q. Q., Yang, W., Wang, F., Bai, Z. P., Zhao, X. D., and Yang, Y. C.: Chemical characterization of submicron aerosol and particle growth events at a national background site (3295 m a.s.l.) on the Tibetan Plateau, Atmos. Chem. Phys., 15, 10811–10824, 10.5194/acp-15-10811-2015, 2015.

Du, W., Zhao, J., Wang, Y., Zhang, Y., Wang, Q., Xu, W., Chen, C., Han, T., Zhang, F., Li, Z., Fu, P., Li, J., Wang, Z., and Sun, Y.: Simultaneous measurements of particle number size distributions at ground level and 260 m on a meteorological tower in urban Beijing, China, Atmos. Chem. Phys., 17, 6797–6811, 10.5194/acp-17-6797-2017, 2017.

Gao, Z., Wang, F., Du, W., Wang, S., Sun, Y., Yang, W., Wang, X., Han, B., and Bai, Z.: Elucidating particle number concentrations and unveiling source mechanisms at a prominent national background site on the northeastern Qinghai-Tibetan Plateau, Sci Total Environ, 969, 178928, 10.1016/j.scitotenv.2025.178928, 2025.

Hakala, S., Vakkari, V., Bianchi, F., Dada, L., Deng, C., Dällenbach, K., Fu, Y., Jiang, J., Kangasluoma, J., and Kujansuu, J.: Observed coupling between air mass history, secondary growth of nucleation mode particles and aerosol pollution levels in Beijing, Environmental science: atmospheres, 2, 146–164, 2022.

Hong, J., Tang, M., Wang, Q., Ma, N., Zhu, S., Zhang, S., Pan, X., Xie, L., Li, G., and Kuhn, U.: Measurement Report: Wintertime new particle formation in the rural area of the North China Plain–influencing factors and possible formation mechanism, Atmospheric Chemistry and Physics, 23, 5699–5713, 2023.

Hu, Y., Yu, H., Kang, S., Yang, J., Rai, M., Yin, X., Chen, X., and Chen, P.: Aerosol–meteorology feedback diminishes the transboundary transport of black carbon into the Tibetan Plateau, Atmospheric Chemistry and Physics, 24, 85–107, 2024.

Hussein, T., Atashi, N., Sogacheva, L., Hakala, S., Dada, L., Petäjä, T., and Kulmala, M.: Characterization of Urban New Particle Formation in Amman—Jordan, 10.3390/atmos11010079, 2020.

Kalivitis, N., Kerminen, V. M., Kouvarakis, G., Stavroulas, I., Tzitzikalaki, E., Kalkavouras, P., Daskalakis, N., Myriokefalitakis, S., Bougiatioti, A., Manninen, H. E., Roldin, P., Petäjä, T., Boy, M., Kulmala, M., Kanakidou, M., and Mihalopoulos, N.: Formation and growth of atmospheric nanoparticles in the eastern Mediterranean: results from long-term measurements and process simulations, Atmos. Chem. Phys., 19, 2671–2686, 10.5194/acp-19-2671-2019, 2019.

https://doi.org/10.5194/egusphere-2026-1628
Preprint. Discussion started: 29 April 2026

Kalkavouras, P., BougiatiotI, A., Hussein, T., Kalivitis, N., Stavroulas, I., Michalopoulos, P., and Mihalopoulos, N.: Regional New Particle Formation over the Eastern Mediterranean and Middle East, 10.3390/atmos12010013, 2021.
Kalkavouras, P., Bougiatioti, A., Kalivitis, N., Stavroulas, I., Tombrou, M., Nenes, A., and Mihalopoulos, N.: Regional new particle formation as modulators of cloud condensation nuclei and cloud droplet number in the eastern Mediterranean, Atmos. Chem. Phys., 19, 6185–6203, 10.5194/acp-19-6185-2019, 2019.
Kalkavouras, P., Bougiatioti, A., Grivas, G., Stavroulas, I., Kalivitis, N., Liakakou, E., Gerasopoulos, E., Pilinis, C., and Mihalopoulos, N.: On the regional aspects of new particle formation in the Eastern Mediterranean: A comparative study between a background and an urban site based on long term observations, Atmospheric Research, 239, 104911, https://doi.org/10.1016/j.atmosres.2020.104911, 2020.
Kerminen, V.-M., Chen, X., Vakkari, V., Petäjä, T., Kulmala, M., and Bianchi, F.: Atmospheric new particle formation and growth: review of field observations, Environmental Research Letters, 13, 103003, 10.1088/1748-9326/aadf3c, 2018.
Kulmala, M., Maso, M. D., Mäkelä, J., Pirjola, L., Väkevä, M., Aalto, P., Miikkulainen, P., Hämeri, K., and O'dowd, C.: On the formation, growth and composition of nucleation mode particles, Tellus B, 53, 479–490, 2001.
Kulmala, M., Petäjä, T., Nieminen, T., Sipilä, M., Manninen, H. E., Lehtipalo, K., Dal Maso, M., Aalto, P. P., Junninen, H., Paasonen, P., Riipinen, I., Lehtinen, K. E. J., Laaksonen, A., and Kerminen, V.-M.: Measurement of the nucleation of atmospheric aerosol particles, Nature Protocols, 7, 1651–1667, 10.1038/nprot.2012.091, 2012.
Lai, S., Qi, X., Huang, X., Lou, S., Chi, X., Chen, L., Liu, C., Liu, Y., Yan, C., Li, M., Liu, T., Nie, W., Kerminen, V. M., Petäjä, T., Kulmala, M., and Ding, A.: New particle formation induced by anthropogenic–biogenic interactions on the southeastern Tibetan Plateau, Atmos. Chem. Phys., 24, 2535–2553, 10.5194/acp-24-2535-2024, 2024.
Lampilahti, A., Garmash, O., Aliaga, D., Arshinov, M., Davydov, D., Belan, B., Lampilahti, J., Kerminen, V.-M., Petäjä, T., Kulmala, M., and Ezhova, E.: Insights into new particle formation in a Siberian boreal forest from nanoparticle ranking analysis, Aerosol Research, 3, 441–459, 10.5194/ar-3-441-2025, 2025.
Li, K., An, Y., Xu, J., Zhong, M., Zhao, W., and Qin, X.: Measurement report: Year-long chemical composition, optical properties, and sources of atmospheric aerosols in the northeastern Tibetan Plateau, Atmospheric Chemistry and Physics, 25, 12433–12450, 2025.
Liu, Y., Nie, W., Qi, X., Li, Y., Xu, T., Liu, C., Ge, D., Chen, L., Niu, G., Wang, J., Yang, L., Wang, L., Zhu, C., Wang, J., Zhang, Y., Liu, T., Zha, Q., Yan, C., Ye, C., Zhang, G., Hu, R., Huang, R.-J., Chi, X., Zhu, T., and Ding, A.: The Pivotal Role of Heavy Terpenes and Anthropogenic Interactions in New Particle Formation on the Southeastern Qinghai-Tibet Plateau, Environmental Science & Technology, 58, 19748–19761, 10.1021/acs.est.4c04112, 2024.
Olin, M., Kuuluvainen, H., Aurela, M., Kalliokoski, J., Kuittinen, N., Isotalo, M., Timonen, H. J., Niemi, J. V., Rönkkö, T., and Dal Maso, M.: Traffic-originated nanocluster emission exceeds H 2 SO 4-driven photochemical new particle formation in an urban area, Atmospheric Chemistry and Physics, 20, 1–13, 2020.
Petters, M. D. and Kreidenweis, S. M.: A single parameter representation of hygroscopic growth and cloud condensation nucleus activity, Atmos. Chem. Phys., 7, 1961–1971, 10.5194/acp-7-1961-2007, 2007.
Rose, C., Sellegri, K., Moreno, I., Velarde, F., Ramonet, M., Weinhold, K., Krejci, R., Andrade, M., Wiedensohler, A., Ginot, P., and Laj, P.: CCN production by new particle formation in the free troposphere, Atmos. Chem. Phys., 17, 1529–1541, 10.5194/acp-17-1529-2017, 2017.
Saha, P. K., Robinson, E. S., Shah, R. U., Zimmerman, N., Apte, J. S., Robinson, A. L., and Presto, A. A.: Reduced Ultrafine Particle Concentration in Urban Air: Changes in Nucleation and Anthropogenic Emissions, Environmental Science & Technology, 52, 6798–6806, 10.1021/acs.est.8b00910, 2018.
Sellegri, K., Rose, C., Marinoni, A., Lupi, A., Wiedensohler, A., Andrade, M., Bonasoni, P., and Laj, P.: New Particle Formation: A Review of Ground-Based Observations at Mountain Research Stations, 10.3390/atmos10090493, 2019.
Shang, D., Hu, M., Zheng, J., Qin, Y., Du, Z., Li, M., Fang, J., Peng, J., Wu, Y., and Lu, S.: Particle number size distribution and new particle formation under the influence of biomass burning at a high altitude background site at Mt. Yulong (3410 m), China, Atmospheric Chemistry and Physics, 18, 15687–15703, 2018.
Shang, D., Tang, L., Fang, X., Wang, L., Yang, S., Wu, Z., Chen, S., Li, X., Zeng, L., Guo, S., and Hu, M.: Variations in source contributions of particle number concentration under long-term emission control in winter of urban Beijing, Environmental Pollution, 304, 119072, https://doi.org/10.1016/j.envpol.2022.119072, 2022.
Shen, L., Wang, H., Yin, Y., Chen, J., and Chen, K.: Observation of atmospheric new particle growth events at the summit of mountain Tai (1534 m) in Central East China, Atmospheric Environment, 201, 148–157, 2019.

https://doi.org/10.5194/egusphere-2026-1628
Preprint. Discussion started: 29 April 2026

Shen, X., Sun, J., Ma, Q., Zhang, Y., Zhong, J., Yue, Y., Xia, C., Hu, X., Zhang, S., and Zhang, X.: Long-term trend of new particle formation events in the Yangtze River Delta, China and its influencing factors: 7-year dataset analysis, Science of The Total Environment, 807, 150783, 2022.

Singh, K., Gautam, A. S., Jeni Victor, N., Kumar, S., Potdar, S. S., Komsaare, K., and Siingh, D.: Characteristics of new particle formation events at high-altitude location of Western Himalayan Region, Tehri Garhwal, India, Atmospheric Research, 315, 107903, https://doi.org/10.1016/j.atmosres.2024.107903, 2025.

Tang, L., Hu, M., Shang, D., Fang, X., Mao, J., Xu, W., Zhou, J., Zhao, W., Wang, Y., Zhang, C., Zhang, Y., Hu, J., Zeng, L., Ye, C., Guo, S., and Wu, Z.: High frequency of new particle formation events driven by summer monsoon in the central Tibetan Plateau, China, Atmos. Chem. Phys., 23, 4343–4359, 10.5194/acp-23-4343-2023, 2023.

Venzac, H., Sellegri, K., Laj, P., Villani, P., Bonasoni, P., Marinoni, A., Cristofanelli, P., Calzolari, F., Fuzzi, S., Decesari, S., Facchini, M.-C., Vuillermoz, E., and Verza, G. P.: High frequency new particle formation in the Himalayas, Proceedings of the National Academy of Sciences, 105, 15666–15671, doi:10.1073/pnas.0801355105, 2008.

Victor, J. N., Buchunde, P., Sebastian, M., Kanawade, V. P., Siingh, D., Mukherjee, S., Potdar, S. S., Dharmaraj, T., and Pandithurai, G.: Characteristics of new particle formation events in a mountain semi-rural location in India, Atmospheric Environment, 324, 120414, https://doi.org/10.1016/j.atmosenv.2024.120414, 2024.

Wang, J., Li, M., Li, L., Zheng, R., Fan, X., Hong, Y., Xu, L., Chen, J., and Hu, B.: Particle number size distribution and new particle formation in Xiamen, the coastal city of Southeast China in wintertime, Science of The Total Environment, 826, 154208, https://doi.org/10.1016/j.scitotenv.2022.154208, 2022.

Wu, H., Li, Z., Jiang, M., Liang, C., Zhang, D., Wu, T., Wang, Y., and Cribb, M.: Contributions of traffic emissions and new particle formation to the ultrafine particle size distribution in the megacity of Beijing, Atmospheric Environment, 262, 118652, https://doi.org/10.1016/j.atmosenv.2021.118652, 2021.

Wu, H., Li, Z., Hai, S., Gao, Y., Jiang, J., Zhao, B., Cribb, M., Zhang, D., Pu, D., Liu, M., Wang, C., Lan, J., and Wang, Y.: Vertical transport of ultrafine particles and turbulence evolution impact on new particle formation at the surface & Canton Tower, Atmospheric Research, 302, 10.1016/j.atmosres.2024.107290, 2024.

Yang, C., Brean, J., Xu, W., Xu, L., Huang, W., Fan, X., Bianchi, F., Du, W., Lin, Z., Li, L., Chen, G., Zhang, Y., Cai, R., Chen, Y., Li, M., and Chen, J.: Anthropogenic Oxygenated Organic Molecules Dominate New Particle Growth in Moderate-Pollution Urban China, Environ Sci Technol, 60, 6364–6377, 10.1021/acs.est.5c11555, 2026.

Yao, L., Garmash, O., Bianchi, F., Zheng, J., Yan, C., Kontkanen, J., Junninen, H., Mazon, S. B., Ehn, M., and Paasonen, P.: Atmospheric new particle formation from sulfuric acid and amines in a Chinese megacity, Science, 361, 278–281, 2018.

Zhang, K., Xu, Z., Zhang, F., and Wang, Z.: Unveiling the organic contribution to the initial particle growth in 3–10 nm size range, Atmospheric Chemistry and Physics, 26, 2241–2254, 10.5194/acp-26-2241-2026, 2026.

Zhang, Q., Jia, S., Yang, L., Krishnan, P., Zhou, S., Shao, M., and Wang, X.: New particle formation (NPF) events in China urban clusters given by sever composite pollution background, Chemosphere, 262, 127842, https://doi.org/10.1016/j.chemosphere.2020.127842, 2021.

Zhao, W., Zhang, X., Zhai, L., Shen, X., and Xu, J.: Chemical characterization and sources of submicron aerosols in Lhasa on the Qinghai–Tibet Plateau: Insights from high-resolution mass spectrometry, Science of the Total Environment, 815, 152866, 2022.